Research Square

Preprints are preliminary reports that have not undergone peer review.
They should not be considered conclusive, used to inform clinical practice,
or referenced by the media as validated information.

Research on tooth surface design and side milling machining method of ruled line face gear

xiaomeng chu (cthzym@buaa.edu.cn)
Liaoning University of Technology
hong zeng
yanzhong wang
yizhan huang

Research Article

Keywords: Face gear, Ruled line, Side milling, Curvature, Tool path generation

Posted Date: July 25th, 2022

DOI: https://doi.org/10.21203/rs.3.rs-1849408/v1

License: This work is licensed under a Creative Commons Attribution 4.0 International License.
Read Full License

Research on tooth surface design and side milling machining method of ruled line face gear

Xiaomeng Chu[1], Hong Zeng[1], Yanzhong Wang[2], Yizhan Huang[2]

1. College of Mechanical Engineering and Automation, Liaoning University of Technology, Jinzhou, China

2. School of Mechanical Engineering and Automation, Beihang University, Beijing, China

Corresponding author:

Xiaomeng Chu, College of Mechanical Engineering and Automation, Liaoning University of Technology, No.169 Shiying Street, Guta Distrcit, Jinzhou, China.

Email: cthzym@buaa.edu.cn

Abstract

In order to solve the problem of generalized design and batch processing of face gear, a method of tooth surface design and side milling of ruled-line face gears is proposed in this paper. First of all, the discrete points of the pitch cone surface of the face gear are calculated, and the straight-line cluster and section curve of the tooth surface are constructed to analyze the deviation of the ruled line face gear. Secondly, the tooth surface model of the ruled line face gear is constructed, and the curvature and contact trace are calculated. Thirdly, the curvature and tangent of the ruled line face gear tooth surface are analyzed, the feed plane of the equidistant surface and the guideline are obtained, the torsion angle of the tooth surface and the distribution of the tangent vector along the generatrix are calculated, and the tool axis position based on the two-point offset method is studied. Finally, the side milling processing test of the face gear is carried out, and the tooth surface of the face gear after side milling is measured. The measurement results verify the correctness of the tooth surface design and the side milling processing method of the ruled line face gear.

Keywords Face gear · Ruled line · Side milling · Curvature · Tool path generation

1 Introduction

Due to its unique technical advantages, face gear transmission has been widely used in more and more fields such as vehicles, aerospace, and ships. The tooth surface of the face gear is a complex curved surface with variable curvature in space, and its design and machining process are complicated, which restricts the pace of its engineering application. In this context, it is urgent to carry out research on the universal design and efficient machining method of face gear tooth surfaces, so as to solve the problem of rapid batch application of face gears.

Many scholars at home and abroad have carried out a lot of research work on the face gear transmission technology. Lin et al. presented a machining method for orthogonal variable ratio face gears using a five-axis CNC machine tool in order to solve manufacturing problems of the face gear [1]. Yang et al. studied a rough machining method for the face-gear through plunge milling and planning, and carried out theoretical research and numerical control simulation machining respectively [2-3]. Shen et al. developed a method of shaving processing for spiroid face gear, the kinematics of the shaving processing was analyzed. And further developed a computer-integrated shaving processing of the gear on a five-axis computer numerical control machine [4-5]. Shih et al. proposed a disk tool cutting method for a five-axis machine whose five-axis coordinates for gear production are derived based on the target tooth surface [6]. Zhou et al. derive an advanced method, based on the geometry characteristic of the tooth surface, to calculate the points as an even distribution on the tooth surface [7]. They present an accurate measurement model of the face gear tooth surface, wherein the digital tooth contact analysis is implemented with a robust algorithm [8].

Peng et al. studied a method where the predesigned contact path and transmission errors are applied to the synthesis of the motion rule, and presented the application of the modern Phoenix bevel gear manufacturing machine tool in the face gear generation by the plane-cutter [9]. Xiang et al. proposes a method to analyze and compensate geometric errors of six-axis CNC grinding machines for spiral bevel gears [10]. Mo et al. studied the changing laws of load

sharing coefficients influenced by flexible support when the sun gear is floating and the sun gear is normally supported [11]. They also studied the multi-power face gear split flow system [12]. Guo et al. presented the procedure of computerized generation and the results of simulation of meshing and stress analysis of face gear drives manufactured by circular cutters without considering the feed motion of the circular cutters, and proposed a kind of approximate definition method of grinding worm surface with variable meshing angle for grinding face gears [13,14].

Dong et al. analyzed the characteristics of dynamic load sharing in a concentric face gear split-torque transmission system, and introduced a concentric face gear torque split system used in the helicopter main transmission to transfer more power and reduce the structure weight [15,16]. Deng et al. presented a machining method referred to as power skiving is applied to the machining of face gears [17]. Wang et al. has done a lot of work on design ang precision machining of face gear. They proposed a precision milling method for face-gear by disk cutter, a precision generating hobbing method for face gear with the assembly spherical hob, a finishing method for the continuous generation of spur face gears with shaving cutters [17-20].

On the basis of the research of the above scholars, this paper proposes a tooth surface design and side milling processing method of ruled line surface gear to solve the complex design and processing problems of the face gear tooth surface. Firstly, the discrete points of the conical surface of the face gear transmission pitch are studied, and the straight line of the face gear tooth surface is constructed. Secondly, the space curvature of the ruled gear is studied, and the tooth surface characteristics of the ruled gear are analyzed. Thirdly, the tool path of ruled-line surface gear machining is studied, and the tool pose planning method is established. Finally, the correctness of the proposed method is verified by the side milling test of ruled gear.

The remainder of Part I of this paper is organized as follows. Sect. 2 provides the tooth surface equation of ruled line face gear. Sect. 3 describes the tooth surface characteristics of ruled line face gear. Sect. 4 describes tool path generation and tool pose planning for ruled line face gear. Sect. 5 conducts the side milling machining test of ruled line face gear. Finally, a Conclusions of the theoretical results is presented in Sect. 6.

2 Tooth surface equation of ruled line face gear

2.1 Discrete points on the cone of face gear

The face gear transmission is a special transmission form by spur gear and bevel gear. In the face gear transmission, there is an instantaneous axis surface equivalent to the pitch cone in the bevel gear transmission.

As shown in Fig. 1, the contact line OI of the two instantaneous axial surfaces is the instantaneous rotary axis in relative motion, and the instantaneous axial surface can be regarded as the line family of the contact line in the respective coordinate systems of the face gear and the pinion. The rotation axis of the face gear is represented by OO_2, the rotation axis of the pinion is represented by OO_s, the r_p is the radius of the indexing circle of the pinion, and the angle between the transmission axis of the involute pinion and the face gear is γ.

The spur gear uses a cylinder with a radius of r as the pitch surface, and the pitch surface of the face gear can be regarded as a conical surface with a half cone apex angle γ_2, and the two pitch surfaces are tangent to the pitch line $O'M$. The intersection of $O'M$ and the tangent OI of the instantaneous axis surface is P, and the face gear and pinion are pure rolling at node P.

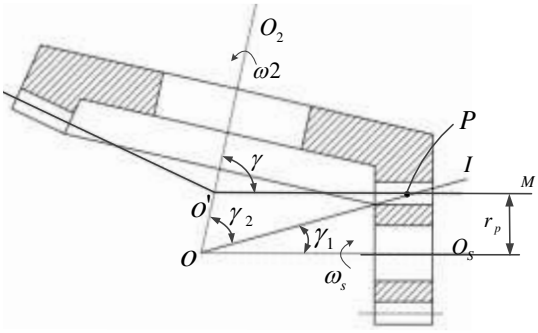

Fig.1 Schematic diagram of face gear transmission

The angle γ_1 between the axis of the spur gear and the instantaneous shaft, and the angle γ_2 between the axis of the face gear and the instantaneous shaft, satisfy the following equations.

$$ctg\gamma_1 = \frac{i_{12} + \cos\gamma}{\sin\gamma} \tag{1}$$

$$ctg\gamma_2 = \frac{i_{21} + \cos\gamma}{\sin\gamma} = \frac{1 + i_{12}\cos\gamma}{i_{12}\sin\gamma} \tag{2}$$

where, $i_{12} = \frac{1}{i_{21}}$.

As shown in Fig. 2, R_1 and R_2 represents the inner and outer radii of the face gear respectively, take any point $P_i(i = 1,2,3...n)$ on the pitch line, and the coordinate of P_i is (R_{2x}, R_{2y}, R_{2z}), then the coordinate of P_i is expressed as

$$\begin{cases} R_{2z} = r_{ps} \\ \sqrt{R_{2x}^2 + R_{2y}^2} = R_i \\ f = n_s v_s^{(2s)} = 0 \\ R_i = R_1 + \frac{i}{n}(R_2 - R_1) \end{cases} \tag{3}$$

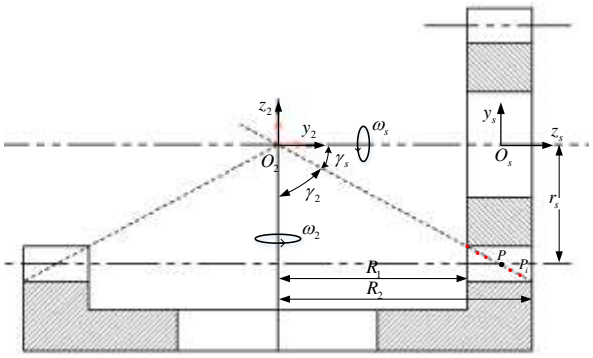

Fig. 2 Schematic diagram of the pitch line of the orthogonal face gear

Discretize the above formula to obtain the set of nodal line points of the face gear, denoted as $R_i\left(i=1,2,3...n\right)$. As shown in Fig. 3, the pitch line is located in the middle part of the face gear tooth surface, and the distance from the tooth top and the tooth root is equal.

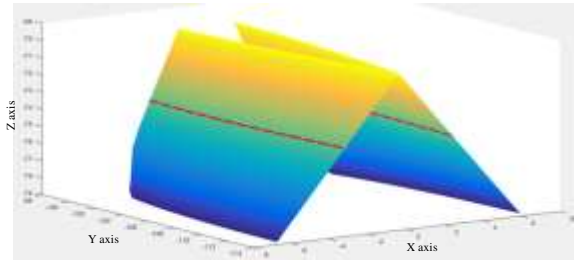

Fig.3 Discrete points of pitch line of face gear

2.2 The straight-line structure of the face gear tooth surface

The face gear tooth surface is intercepted by plane $y=y_0$ parallel to the y-axis, and the curve $y=y_0$ of the intersection of the face gear tooth surface and l_2 is obtained.

$$\begin{cases} x=x\left(u,t\right) \\ y=y\left(u,t\right) \\ z=z\left(u,t\right) \\ y=y_0 \end{cases} \tag{4}$$

According to the above formula, the section curve l_2 of the face gear can be obtained. In order to further analyze the bending degree of the curve l_2, the curvature q of each point on the curve is calculated.

$$\begin{cases} q=\dfrac{\left|r^{'}\left(t\right)-r^{''}\left(t\right)\right|^2}{\left|r^{'}\left(t\right)\right|^3} \\ r\left(t\right)=t\left(x\left(u,t\right),y\left(u,t\right),z\left(u,t\right)\right) \\ y\left(u,t\right)=y_0 \end{cases} \tag{5}$$

The modulus of the face gear is 4, the pressure angle is 25°, the number of teeth of the gear shaper and the face gear are 37 and 51 respectively, the inner and outer radii are 97.3mm and 112.2mm respectively, and the coordinates of the tooth top and tooth bottom are -70mm and -79mm respectively.

When $y_0=115$ mm, the curvature of the discrete points of the cross-section curve is obtained according to formulas (4) and (5). The calculation results are shown in Fig.4. The maximum curvature at the tooth top is 0.0015, and the minimum curvature at the tooth bottom is 2.43×10^{-4}.

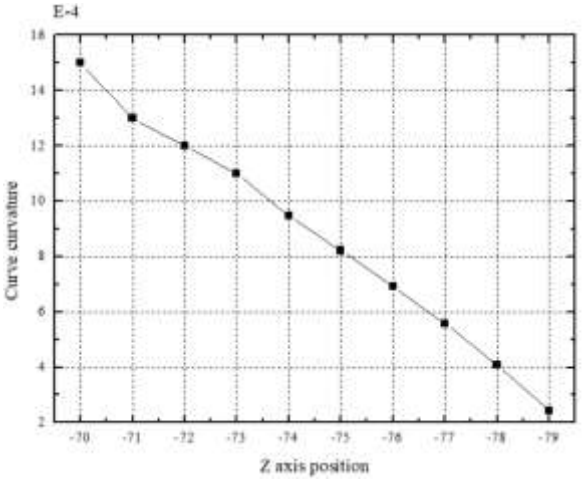

Fig. 4 Curvature of the cross-section curve

It can be seen from the above calculation that the curvature of the face gear section along the Y-axis is approximately 0, so the curve on the face gear section can be approximately regarded as a straight line, and the starting points of the straight-line segment are the tooth tip and the tooth root respectively.

The calculation formula of discrete point $P_{a,m}$ of tooth tip and tooth root is as follows.

$$\begin{cases} R_{2z}=r_{a,m} \\ R_{2y}=R_i \\ f=n_s v_s^{(2s)}=0 \\ R_i=R_1+\dfrac{i}{n}\left(R_2-R_1\right) \end{cases} \tag{6}$$

where, $i=\left(1,2,3...n\right)$.

The equation of the straight line passing through the two points of the tooth tip and the tooth root is as follows.

$$\frac{x-x_a}{x_m-x_a}=\frac{y-y_a}{y_m-y_a}=\frac{z-z_a}{z_m-z_a} \tag{7}$$

Thus, the family of straight-line equations Σ_1 is obtained, as shown in Fig.5.

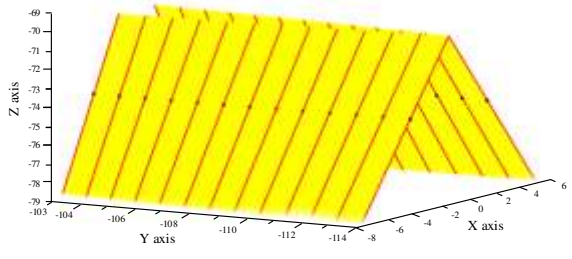

Fig. 5 Line family on face gear

2.3 Face Gear Tooth Surface Line Family and Corresponding Section Curve

Let y and z take discrete values along the direction of tooth height and tooth length respectively, and obtain the corresponding point $R_2(x_2, y_2, z_2)$ on the cross-section curve of the face gear and point $R_l(x_l, y_l, z_l)$ on the straight line.

$$\begin{cases} y = R_{\min} + (R_{\max} - R_{\min})\dfrac{i}{n} \\ z = -\left(z_{rm} + (z_{ra} - z_{rm})\dfrac{i}{n}\right) \\ f(x_2, y_2, z_2) = n_s v_s^{(2s)} = 0 \\ \dfrac{x_l - x_a}{x_m - x_a} = \dfrac{y - y_a}{y_m - y_a} = \dfrac{z - z_a}{z_m - z_a} \end{cases} \tag{8}$$

Thus, the distance d between the discrete points on the section curve and the corresponding points on the construction line is

$$d = \left|\overrightarrow{R_2} - \overrightarrow{R_l}\right| \tag{9}$$

The distance from the straight line of the meshing area to the tooth surface is shown in Fig.6. The largest deviation occurs in the pitch line part, which is 0.015mm.

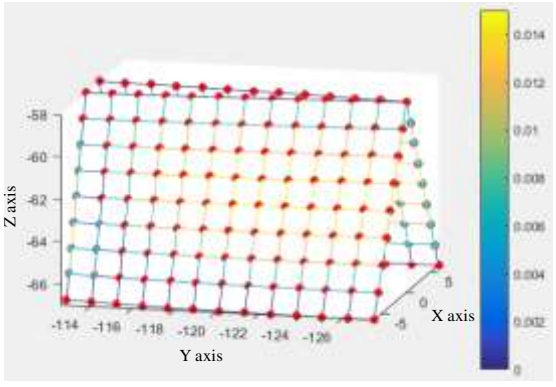

Fig. 6 Distance from the straight line of the meshing area to the tooth surface

2.4 Deviation Analysis of Linear Constructed Face Gear

The ruled lines constructed on the face gear are discretized, and the deviation of the two surfaces is analyzed by comparing the new surface with the theoretical face gear. The face gear tooth surface points are discretized according to (9×15) along the direction of tooth width and tooth height, as shown in the following aquations.

$$\begin{cases} z^{(1,2)}{}_{(\varphi,\theta)} = rm + (ra - rm)\dfrac{k}{9} \\ y^{(1,2)}{}_{(\varphi,\theta)} = R_1 + \dfrac{j}{15}(R_2 - R_1) \\ x^{(1,2)} = x_{(\varphi,\theta)} \end{cases} \tag{10}$$

The tooth surface deviation d_f is expressed as the normal distance between discrete points P_1 and P_2 as

$$d_f = \left|\overrightarrow{P_1P_2}\right|\cos(\alpha) \tag{11}$$

where, α is the angle between the normal line of the face gear tooth surface point at point P_2 and the vector $\overrightarrow{P_1P_2}$.

The fitting deviation results of the theoretical surface and the structural surface of the face gear are shown in Fig.7. The maximum normal deviation between the constructed linear face gear and the theoretical face gear is 0.0204mm, which appears in the pitch line local area.

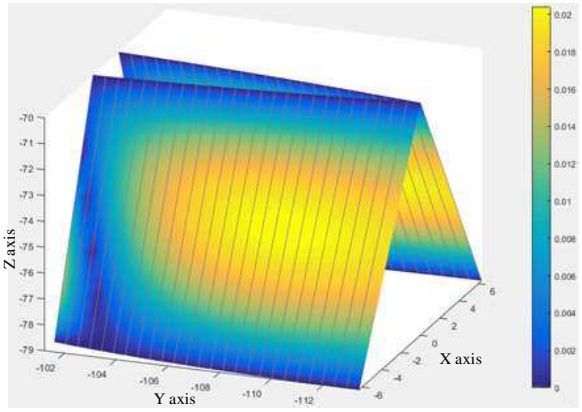

Fig.7 Fitting deviation between theoretical surface and structural surface of face gear

3 Tooth surface characteristics of ruled line face gear

3.1 Ruled line face gear tooth surface model

The tooth surface of the face gear is a space surface composed of involutes and angle parameters. The equation of surface can be expressed as

$$\vec{r}_2(u,t) = \vec{r}_a(y) + \vec{l}(u,t) \tag{12}$$

where, $\vec{a}(y)$ represents the intersection vector of the cross section and the tooth top along the y axis, and $\vec{l}(u,t)$ represents the unit vector from the tooth top to the P point of the tooth surface along the cross-section direction.

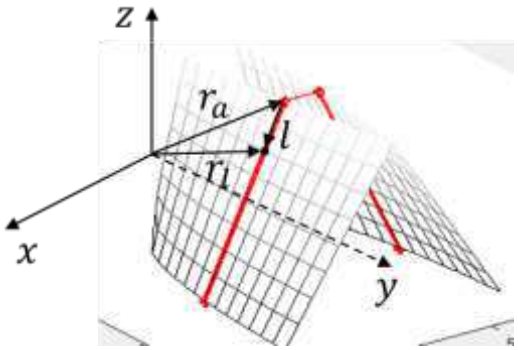

Fig. 8 Vector representation of tooth flank points of face gear

According to Fig.8, the tooth surface equation of the ruled line face gear can be expressed as

$$\begin{cases} \vec{r}_l(u,t) = \vec{r}_a(y) + \vec{l}(u,t) \\ \vec{l}(u,t) = v\vec{l}(y) \end{cases} \tag{13}$$

$$\vec{r}_a(y) = \begin{Bmatrix} x(y) = r_2(u(y),t(y)) \\ y = y(u,t) \\ z(u,t) = -r_a \end{Bmatrix} \tag{14}$$

Further, the tooth surface equation of the ruled line face gear can be obtained. It can be seen from the above formula that the face gear tooth surface is a ruled surface, the generatrix of the ruled surface is $\vec{l}(y)$, and the directrix is $\vec{r}_a(y)$. The three-dimensional model of the ruled line face gear is thus obtained as shown in Fig.9.

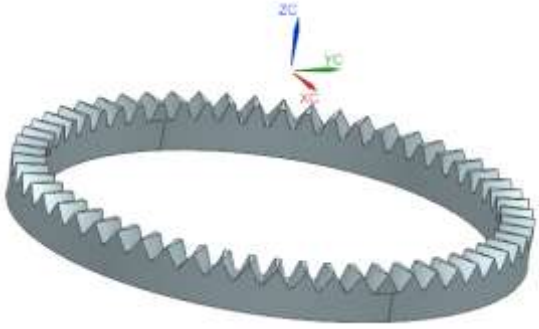

Fig. 9 3D model of ruled line face gear

3.2 Spatial curvature comparison between ruled line surface and theoretical tooth surface

The tooth surface of the face gear can be expressed as the surface $r(\varphi_s,\theta_s)$, then the normal vector of any point P on the surface is expressed as

$$\vec{n}_p = \frac{\vec{r}_{\varphi_s} \times \vec{r}_{\theta_s}}{\left|\vec{r}_{\varphi_s} \times \vec{r}_{\theta_s}\right|} \tag{15}$$

where, $\vec{r}_{\varphi_s}$ is the partial derivative of the surface with respect to φ_s, and $\vec{r}_{\theta_s}$ is the partial derivative of the surface with respect to θ_s.

$$K = \frac{Ld\varphi_s^2 + 2Md\varphi_s d\theta_s + Nd\theta_s^2}{Ed\varphi_s^2 + 2Fd\varphi_s d\theta_s + Gd\theta_s^2} \tag{16}$$

Further, the calculation formula of normal curvature can be obtained as

$$\left(EG - F^2\right)K^2 + \left(2FM - EN - GL\right)K + \left(LN - M^2\right) = 0 \tag{17}$$

Thus, the main curvatures $K1$ and $K2$ of the ruled line face gear can be obtained. Further, the face gear tooth surface point coordinates are discretized, and the principal curvature of the tooth surface corresponding to each discrete point is calculated to obtain the face gear curvature distribution cloud diagram as shown in Fig.10.

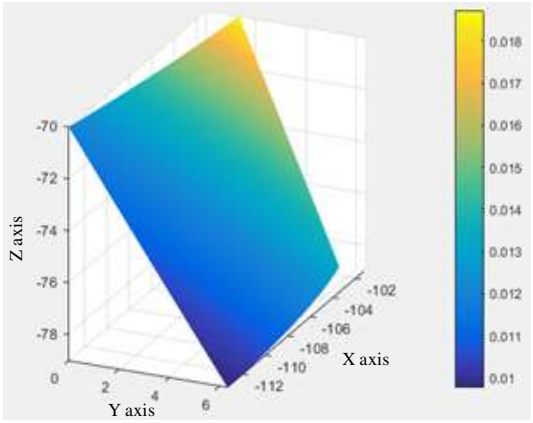

(a) Principal curvature $K1$ of the tooth flank

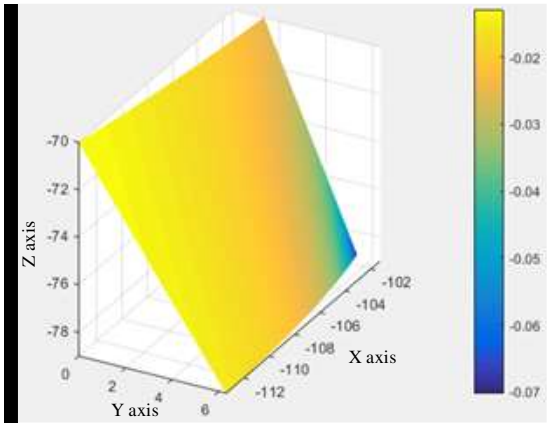

(b) Principal curvature $K2$ of the tooth flank

Fig.10 Main curvature distribution of face gear

3.3 Representation of the contact trace of the ruled line face gear

The meshing coordinate system of the ruled line face gear is established as shown in Fig.11. $S_{p0}\left(x_{p0},y_{p0},z_{p0}\right)$ and $S_{g0}\left(x_{g0},y_{g0},z_{g0}\right)$ are the fixed coordinate systems of pinion

and ruled line face gear, $S_p\left(x_p, y_p, z_p\right)$ and $S_g\left(x_g, y_g, z_g\right)$ are the rotational coordinate systems of pinion and ruled line face gear. γ is the axis angle of the ruled line face gear and the pinion, $\gamma = 90^{\circ}$. φ_1, φ_2 are the rotation angles of the pinion and the ruled line face gear, respectively.

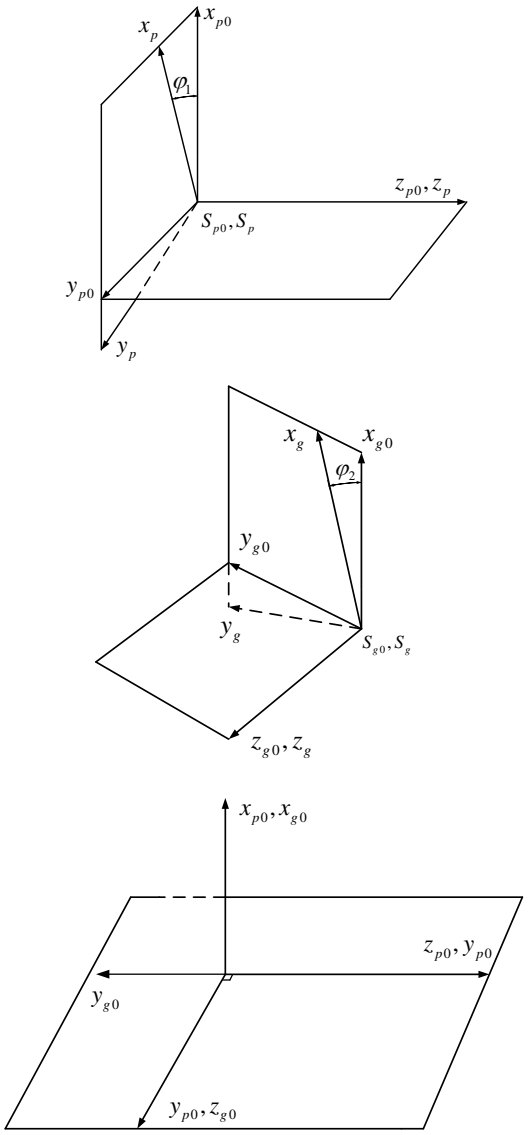

Fig. 11 Meshing coordinate system of ruled line face gear

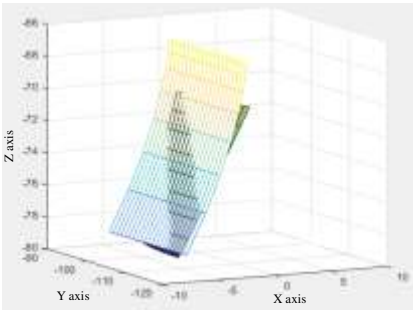

(a) $\varphi_1 = 0^{\circ}$

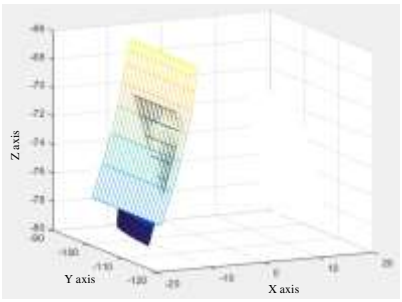

(b) $\varphi_1 = 4^{\circ}$

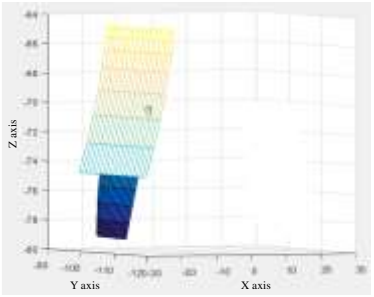

(c) $\varphi_1 = 9^{\circ}$

Fig. 12 Discrete visualization of meshing process

The position and normal vectors of the face gear and pinion at the meshing point are

$$r_l^{(1)}\left(u, \varphi_1\right) = r_p^{(2)}\left(\theta_2 \varphi_2 z_2\right) \tag{18}$$

$$n_l^{(1)}\left(u, \varphi_1\right) = n_g^{(2)}\left(\theta_2 \varphi_2 \varphi_2^{'}\right) \tag{19}$$

Visualize the actual meshing process of the ruled line face gear and the pinion. As shown in Fig.12, the meshing process of the ruled line face gear and the pinion belongs to the form of line contact, and the contact line coincides with the direction of the contact trace.

4 Tool path generation and tool pose planning for ruled line face gear

4.1 Alignment curvature and tangent vector of ruled line face gear

The directrix $\overset{\mathbf{u}}{r}_a(y)$ of the ruled line face gear can be regarded as the intersection line of the tooth top plane and the tooth surface of the theoretical face gear. The tangent vector of the directrix is

$$\overset{\mathbf{u}}{r}^{'}(y) = \begin{Bmatrix} \dfrac{\partial x}{\partial u}\dfrac{\partial u}{\partial t}\dfrac{\partial t}{\partial y} + \dfrac{\partial x}{\partial t}\dfrac{\partial t}{\partial y} \\ 1 \\ 0 \end{Bmatrix} \tag{20}$$

By discretizing the points on the directrix, the tangent vector of the upper and lower directrix on the tooth surface of the ruled line face gear can be obtained, as shown in Fig.13.

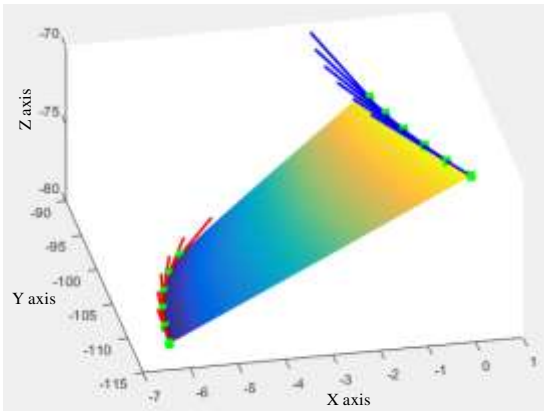

Fig. 13 Tangent vector of ruled line face gear alignment

Further calculate the curvature of the directrix on the ruled line face gear, as shown in Fig.14. The curvature calculation result is between the interval $(0.01,0.06)$, and the curvature change is stable and small.

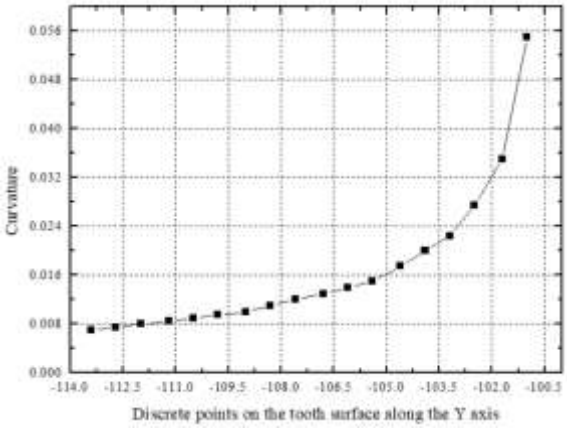

Fig. 14 Alignment curvature of ruled line face gear

4.2 Equidistant surface and feed plane of directrix

Given the maximum error ε, construct equidistant tooth surfaces $s_{\varepsilon 1}(u1,t1)$ and $s_{\varepsilon 2}(u2,t2)$ parallel to the tooth surface and with a distance ε along the normal direction of the ruled line face gear. The tooth surface of the ruled line face gear is $s(u,t)$, and the normal vector is $n(u,t)$, then the equidistant tooth surface equation is

$$s_{\varepsilon i}(u,t)=s(u,t)\pm\varepsilon n(u,t) \tag{21}$$

Any point P_k on the directrix L_j is the theoretical tangent point, and the tangent l_j of the curve L_j through P_k, the plane formed by the tangent l_j and the normal vector $n_k(u,t)$ of the P_k point is the feed plane $\sum$ of the tool, as shown in the following equation.

$$\overrightarrow{PP_k}\cdot n(u,t)=0 \tag{22}$$

The two equidistant surfaces of the ruled line tooth surface are determined by the maximum error, which limits the maximum range of the actual machining path movement of the tool. Within this motion range, the fewer contact points, the less the number of interpolation motions in the actual machining process, and the higher the machining efficiency. The feed plane represents the direction of the tool's interpolated movement.

The constant-bow height error variable-step interpolation is adopted, the maximum arc-height error is set to 0.005mm, the alignment line l on the tooth surface of the ruled line face gear is selected, and the constant-bow height error method is used to discretize the curve. In order to meet the maximum bow height error, the discrete distance is selected as 0.129, and there are 124 discrete points in total, and the tooth surface alignment is discrete. The discrete results are shown in Fig.15.

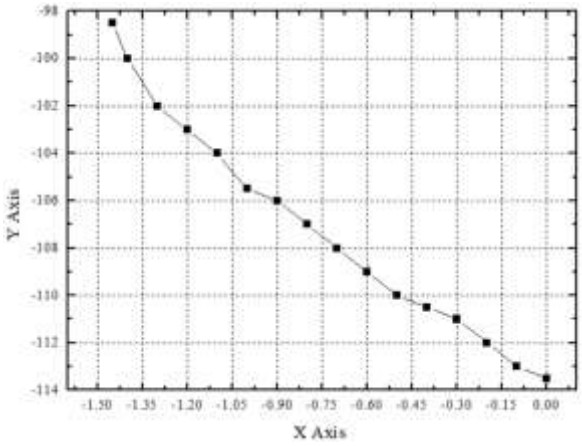

Fig. 15 Directive isoparameter discrete method

The result error calculation of isoparameter discreteness is shown in Fig.16. Under the variable step length and equal bow height error, the bow height error of each interpolation point satisfies the maximum allowable error.

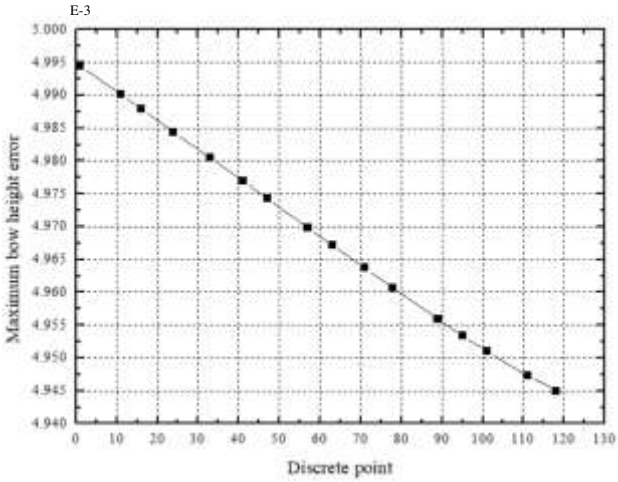

Fig. 16 Equal bow height error distribution

4.3 The torsion angle and generatrix tangent of the ruled

line face gear

The angle between the tangent vector between the busbar and the intersection of the upper and lower directrix is shown in the following equation.

$$\theta = \arccos\left(\frac{|a||b|}{|a \cdot b|}\right) \tag{23}$$

As shown in Fig.17, the intersection points of the same generatrix parameter and the upper and lower directrix lines are P_{t1} and P_{t2} respectively. The tangent vectors $\vec{l}_{1t}$ and $\vec{l}_{2t}$ of the directrix are made through P_{t1} and P_{t2}, and the $\vec{l}_{1t}$ is translated to P_{t2}. The angle θ between the two vectors is the torsion angle of the tooth surface.

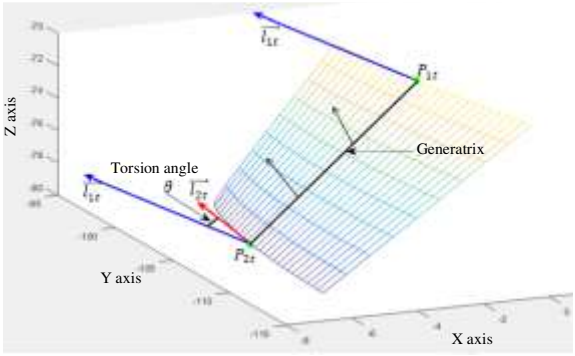

Fig. 17 Torsion angle of tooth surface

The normal vector of the ruled line face gear can be expressed as

$$\begin{cases} \dfrac{\partial \vec{r}}{\partial u} = \vec{l}(y) \\ \dfrac{\partial \vec{r}}{\partial y} = \dfrac{\partial \vec{r}_a(y)}{\partial y} + u\dfrac{\partial \vec{l}(y)}{\partial y} \\ \vec{n} = \dfrac{\partial \vec{r}}{\partial y} \times \dfrac{\partial \vec{r}}{\partial u} \end{cases} \tag{24}$$

Calculate the normal vectors $\vec{n}$ of discrete point positions along a generatrix, and the calculation results are shown in Fig.18.

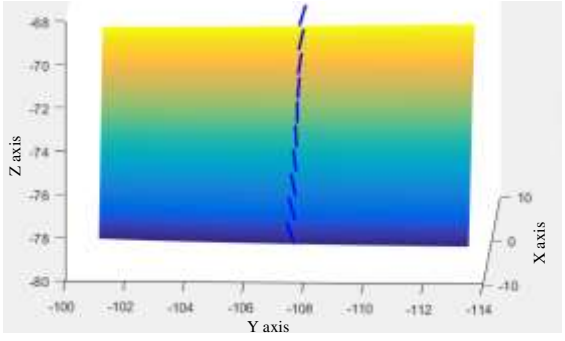

Fig. 18 Generatrix normal vector

It can be seen from the above figure that for a generatrix corresponding to the same parameter y, the normal vector of each discrete point along the generatrix is not in the same plane, and the resulting machining error is shown in Fig.19.

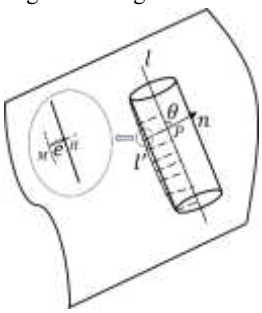

Fig. 19 Mapping curve and machining deviation

The axis of the tool tooth surface is l, a point on the tool axis is P, and the tool is projected to the tooth surface along the normal vector $\vec{n}$ through the point P. The intersection of the normal vector $\vec{n}$ and the tool axis is θ, the projection point is M, and the intersection of the projection vector and the tooth surface is H. $\vec{MH}$ represents the corresponding machining error, the size of $\vec{MH}$ represents the size of the error, the positive direction represents the residual, and the negative direction represents the overcut, as shown in the following equation.

$$\vec{MH} = \frac{r}{\sin(\theta)} - \vec{MP} \tag{25}$$

4.4 Tool axis pose planning based on two-point offset method

The principle of the two-point offset method is shown in Fig.20. Select the generatrix $P_{1t}P_{2t}$ corresponding to a certain parameter on the ruled surface, P_{1t} and P_{2t} are respectively two points on the guideline, and two points Q_{t1} and Q_{t2} are arbitrarily selected on the generatrix. Offset the radius r along the normal vectors $\vec{n}_{t1}$ and $\vec{n}_{t2}$ respectively, then the tool axis vector is

$$\vec{c} = \vec{O_{t1}O_{t2}} = -Q_{t1}(y) + Q_{t2}(y) - r\vec{n}_{t1}(y) + r\vec{n}_{t2}(y) \tag{26}$$

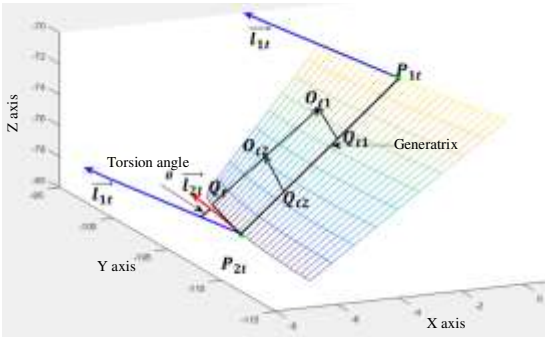

Fig. 20 Tool path double-point offset method

The projection point Q_t of the lower guideline point P_{2t} to $\vec{c}$ is the tool nose point, and the position vector of the tool axis can be determined according to Q_t and the tool axis vector $\vec{c}$. Take 0.25 and 0.75 of the directrix along the reference point in the direction of the directrix, and obtain the axis pose of each interpolation point according to the directrix interpolation method, as shown in Fig.21.

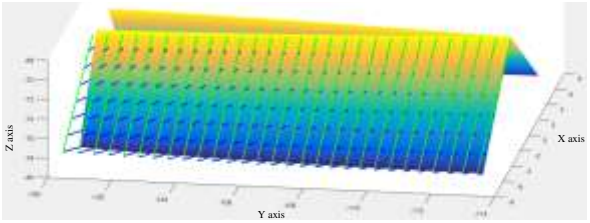

Fig. 21 Tool path pose based on two-point offset

5 Side milling machining test of ruled line face gear

Under the guidance of the above research, the NC machining program was compiled, and the side milling test of ruled line gear was carried out on the J1VMC540W five-axis linkage machine tool. The spindle speed was set to 3000r/min, the feed rate was 0.1mm, and the processing method was down milling. The side milling process is shown in the Fig. 22. The three-coordinate measuring machine is used to test the tooth surface of the face gear after processing. The test results are shown in the Fig. 23. It can be seen from the figure that the maximum deviation occurs at the undercut of the inner diameter tooth bottom, which is 0.02mm, which meets the accuracy requirements.

Fig. 22 Side milling of ruled line face gear

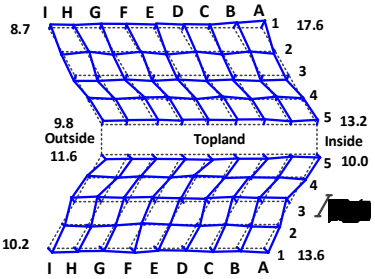

Fig. 23 Tooth surface measurement results

6 Conclusion

In order to effectively improve the design and machining efficiency of face gears, a method of tooth surface design and side milling of ruled-line face gears is proposed in this paper. Firstly, through the structure of discrete points and straight-line clusters on the face gear tooth surface, the tooth surface equation and deviation analysis method of the ruled line surface gear are established. Secondly, according to the mathematical model of the tooth surface of the ruled gear, the characteristics of the tooth surface of the face gear are studied, and the method of representing the contact trace of the ruled gear is established. Thirdly, the tool path of the ruled gear is established, and the tool path planning is completed. The simulation results show the correctness of the planning method. Finally, under the guidance of the theory and simulation results, the side milling processing test of the ruled line gear was carried out. The maximum deviation of the gear detection after processing was 0.017mm, which verifies the correctness of the design and processing method.

Author contribution Xiaomeng Chu contributed to the conception of the study, wrote the manuscript, funding acquisition ; Hong Zeng contributed to the conception of the study and manuscript review; Yanzhong Wang contributed to analysis and manuscript review; Yizhan Huang contributed to the experimental verification..

Funding This work was supported by the basic Scientific Research Project of Liaoning Higher Education Institutions of the Education Department (Grant No. LJKZ0603).

Declarations

Ethics approval Not applicable.

Consent to participate The authors have consent to participate.

Consent to publish The authors have consent to publish.

Competing interests The authors declare no competing interests.

References

1. Lin C, Fan Y, Wang Y, Cao XJ, Cai ZQ (2014) A five-axis CNC machining method of orthogonal variable transmission ratio face gear. J Adv Mech Des Syst 8(3): JAMDSM0040-JAMDSM0040.
2. Yang X Y, Tang J Y (2014) Research on manufacturing method of CNC plunge milling for spur face-gear. Journal of Materials

Processing Tech 214(12):3013-3019.

3. Tang JY, Yang XY (2016) Research on manufacturing method of planning for spur face-gear with 4-axis CNC planer. Int J Adv Manuf Technol 82(5-8):847-858.
4. Shen YB, Liu X, Li ZP, Li DY (2017) Research on shaving processing of spiroid face gear. Int J Adv Manuf Technol 92:605–613.
5. Shen YB, Liu X (2018) Computer-integrated shaving processing for spiroid face gear on a five-axis CNC machine. Int J Adv Manuf Technol 97:1061–1070.
6. Shih YP, Sun ZH, Wu FC (2018) A disk tool cutting method for bevel gear manufacture on a five-axis machine. Int J Adv Manuf Technol 94:855–865.
7. Wu YH, Zhou YS, Zhou ZY, Tang JY, Ouyang HW (2018) An advanced CAD/CAE integration method for the generative design of face gears. Adv Eng Softw 126:90-99.
8. Wang SH, Zhou YS, Tang JY, Tang K, Li ZMQ (2022) Digital tooth contact analysis of face gear drives with an accurate measurement model of face gear tooth surface inspected by CMMs. Mech Mach Theory 167:104498.
9. Peng XL, Niu QY, Guo W, Fang ZD (2018) A New Method of Motion Rule Synthesis for Face Gear Manufacturing by Plane-Cutter. ASME. J. Mech. Des 140(2): 023302.
10. Xiang ST, Li HM, Deng M, Yang JG (2018) Geometric error analysis and compensation for multi-axis spiral bevel gears milling machine. Mech Mach Theory 121:59-74.
11. Mo S, Zhang T, Jin GG, Cao XL, Gao HJ (2020) Analytical Investigation on Load Sharing Characteristics of Herringbone Planetary Gear Train with Flexible Support and Floating Sun Gear. Mech Mach Theory 144 (2):1-27.
12. Mo S, Yue ZX, Feng ZY, Shi LJ, Zou ZX, Dang HY (2020) Analytical investigation on load-sharing characteristics for multi-power face gear split flow system. J Mech Eng Sci 234 (2):676-692.
13. Guo H, Gonzalez-Perez I, Fuentes-Aznar A (2019) Computerized generation and meshing simulation of face gear drives manufactured by circular cutters - ScienceDirect. Mech Mach Theory 133:44-63.
14. Guo H, Zhang SY, Wu TP, Zhao N (2021) An approximate design method of grinding worm with variable meshing angle and grinding experiments of face gear. Mech Mach Theory 166:104461.
15. Dong JX, Wang QB, Tang JY, Hu ZH, Li XQ (2021) Dynamic characteristics and load-sharing performance of concentric face gear split-torque transmission systems with time-varying mesh stiffness, flexible supports and deformable shafts[J]. Meccanica 56:2893-2918.
16. Dong JX, Hu ZH, Tang JY, Wang ZW, Chen SY (2021) Investigation of the Vibration Features and Dynamic Load Sharing Characteristics of Concentric Face Gear Torque Split Transmission. J Comput Nonlin Dyn 16(7):071003.
17. Han ZY, Jiang C, Deng XZ (2022) Machining and meshing analysis of face gears by power skiving. J Adv Mech Des Syst 16(1): JAMDSM0002.
18. Wang YZ, Hou LW, Lan Z, Zhu CL (2017) Precision milling method for face-gear by disk cutter. Int J Adv Manuf Technol 89:1545–1558 .
19. Wang YZ, Chu XM, Zhao WJ, Wang Z, Su GY, Huang YZ (2019) A precision generating hobbing method for face gear with assembly spherical hob. J Cent South Univ 26(10):2704-2716.
20. Wang YZ, Su GY, Chu XM, Huang YZ, E SY, Zhang W, Liu Y (2021) A finishing method for the continuous generation of spur face gears with shaving cutters, Int J Mech Sci 190:106020,